

# Zero-Shot Metric Depth with a Field-of-View Conditioned Diffusion Model

Saurabh Saxena<sup>†</sup>, Junhwa Hur<sup>‡</sup>, Charles Herrmann<sup>‡</sup>, Deqing Sun<sup>‡</sup>, David J. Fleet<sup>†\*</sup>  
<sup>†</sup>Google DeepMind   <sup>‡</sup>Google Research

{srbs, junhwahur, irwinherrmann, deqingsun, davidfleet}@google.com

## Abstract

While methods for monocular depth estimation have made significant strides on standard benchmarks, zero-shot metric depth estimation remains unsolved. Challenges include the joint modeling of indoor and outdoor scenes, which often exhibit significantly different distributions of RGB and depth, and the depth-scale ambiguity due to unknown camera intrinsics. Recent work [5] proposed a specialized multi-head architecture for jointly modeling indoor and outdoor scenes. In contrast, we advocate a generic, task-agnostic diffusion model, with several advancements such as log-scale depth parameterization to enable joint modeling of indoor and outdoor scenes, conditioning on the field-of-view (FOV) to handle scale ambiguity and synthetically augmenting FOV during training to generalize beyond the limited camera intrinsics in training datasets. Furthermore, by employing a more diverse training mixture than is common, and an efficient diffusion parameterization, our method, Diffusion for Metric Depth (DMD) achieves a 25% reduction in relative error (REL) on zero-shot indoor and 33% reduction on zero-shot outdoor datasets over the current SOTA [5] using only a small number of denoising steps. For an overview see [diffusion-vision.github.io/dmd](https://diffusion-vision.github.io/dmd)

## 1. Introduction

Monocular estimation of metric depth in general environments, while useful for applications such as mobile robotics and autonomous driving, has proven elusive. The two main barriers stem from (1) the large differences in RGB and depth distributions one finds in indoor and outdoor datasets, and (2) intrinsic scale ambiguity in images when one lacks knowledge of camera intrinsics. Not surprisingly, most current models for monocular depth are either specific to indoor or outdoor scenes, or, if trained for both, they estimate scale-invariant depth.

Current models for metric depth are often trained solely on indoor or outdoor scenes, primarily on a single dataset captured with fixed camera intrinsics (e.g., with an RGBD

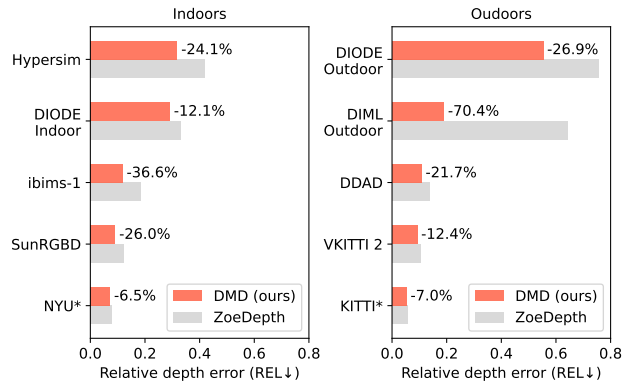


Figure 1. Relative depth error for DMD (ours) compared to ZoeDepth (SOTA) on eight zero-shot and two in-distribution (\*) benchmarks. DMD outperforms ZoeDepth by a substantial margin on all benchmarks.

camera, or, with RGB+LIDAR for outdoor scenes). Such models avoid challenges caused by different indoor and outdoor depth distributions, but at the cost of generality. They also overfit to the camera intrinsics of the training dataset and do not generalize well to out-of-distribution data.

The predominant approach to jointly modeling indoor and outdoor data is to estimate scale- and shift-invariant depth, rather than metric depth (e.g., MiDaS [34]). By normalizing the depth distributions, one brings indoor and outdoor depth distributions closer, and also avoids the problems of scale ambiguities in the presence of variable camera intrinsics. Recently there has been growing interest in bridging these different approaches, training joint indoor-outdoor models that estimate metric depth. To cope with both indoor and outdoor domains, ZoeDepth [5] adds two heads to MiDaS [34], one for each domain, to convert from scale-invariant depth to metric depth.

In this paper we advocate denoising diffusion models for zero-shot metric depth estimation, with the aid of several key innovations to obtain state-of-the-art performance. In particular, field-of-view (FOV) augmentation is used during training to improve generalization to different camera intrinsics, and FOV conditioning in training and inference helps to resolve intrinsic scale ambiguities, providing a fur-

\*DF is also affiliated with the University of Toronto and the Vector Institute.

ther boost in performance. Representing depth in the log domain allocates model capacity in a more balanced way for indoor and outdoor scenes, improving indoor performance. Finally, we find that  $v$ -parameterization in neural network denoising greatly increases inference speed. The resulting model, dubbed DMD (Diffusion for Metric Depth), outperforms recently proposed metric depth model, ZoeDepth [5]. In particular, DMD yields much lower relative depth error than ZoeDepth on all eight out-of-distribution datasets in [5] when fine-tuned on the same data. Expanding the training dataset leads to further improvement in performance (Fig. 1).

To summarize, we make the following contributions:

- We introduce DMD, a simple yet effective method for zero-shot metric depth estimation on general scenes.
- We propose synthetically augmenting the FOV for improved generalization, FOV conditioning to resolve depth-scale ambiguity and representing depth in log-scale to better utilize the model’s representation capacity.
- DMD establishes a SOTA on zero-shot metric depth, achieving 25% and 33% lower relative error than ZoeDepth on indoor and outdoor datasets, respectively, while being efficient, owing to the use of  $v$ -parameterization for diffusion.

## 2. Related Work

**Monocular depth (fine-tuned and evaluated in-domain).** Given the challenges of learning a joint indoor-outdoor model, most approaches have restricted models to target a single dataset (either indoor or outdoor) with fixed intrinsics. In this setting, great progress has been made with advancements in specialized architectures [15, 16] such as the use of binning [1, 3, 8, 18, 30] or loss functions [15, 28] that are suited for this task. [2] proposed combining multiple training datasets with variable intrinsics by normalizing the images to the same camera intrinsic.

**Joint indoor-outdoor models.** To train joint indoor-outdoor models, one can mitigate the difficulty of learning diverse scene statistics by estimating scale- and shift-invariant depth instead. MiDaS [34] trains their model on diverse indoor-outdoor datasets and demonstrates good generalization to various unseen datasets. However, they do not provide metric depth. DPT [35] leverages this for pre-training and further fine-tunes separately for metric depth on NYU and KITTI. ZoeDepth [5] proposes adding a mixture-of-experts head, supervised by scene type, on top of a similarly pre-trained model, thereby handling indoor and outdoor scenes. In contrast, our model, DMD, uses a relatively generic framework, without domain-specific architectural components.

**Intrinsics-conditioned monocular depth.** Incorporating camera intrinsics for depth estimation has been briefly ex-

plored in previous work [17, 22]. They argue that intrinsic-conditioning allows one to train on multiple datasets with varying intrinsics, but this is only demonstrated with small-scale experiments. Similar to our method, ZeroDepth [21] introduces an intrinsic-conditioned metric-scale depth estimator that is trained on large-scale training datasets.

While conditioning on the input field-of-view, we introduce a novel field-of-view augmentation scheme that augments training data by cropping or uncropping to simulate diverse FOVs and provide a large scale study on zero-shot generalization to both indoor and outdoor domains as well as robustness to diverse camera intrinsics.

**Diffusion for vision.** Denoising diffusion models [23, 43] have recently emerged as a powerful class of generative models. Although initially proposed for natural image generation [13, 24, 32, 38], they have recently been shown to be effective for several computer vision tasks such as semantic segmentation [26], panoptic segmentation [9], optical flow [40] and monocular depth estimation [14, 26, 40]. Ours is the first demonstration that diffusion models can also support state-of-the-art zero-shot metric depth estimation for general indoor or outdoor scenes.

## 3. Diffusion for Metric Depth (DMD)

In what follows we describe DMD (Diffusion for Metric Depth) and the design decisions to solve these issues. In particular, we cast monocular depth estimation as a **generative RGB-to-depth translation task using denoising diffusion**. To this end we introduce several technical innovations to conventional diffusion models and training procedures to **accommodate zero-shot, metric depth**.

### 3.1. Diffusion models

Diffusion models are probabilistic models that assume a forward process that gradually transforms a target distribution into a tractable noise distribution. A learned neural denoiser is trained to reverse this process, iteratively converting a noise sample to a sample from the target distribution. They have been shown to be remarkably effective with images and video, and they have recently begun to see use for dense vision tasks like segmentation, tracking, optical flow, and depth estimation. They are attractive as they exhibit strong performance on regression tasks, capturing posterior uncertainty, without task specific architectures, loss functions and training procedures.

For DMD we build on the **task-agnostic Efficient U-Net architecture from DDVM** [40]. While DDVM used the  $\epsilon$ -parameterization for training the neural depth denoiser, here instead we use the  **$v$ -parameterization** [39]. We find that the  $v$ -parameterization yields remarkably efficient inference, using as few as one or two refinement steps, without requiring **progressive distillation** [39].

Under the  $v$ -parameterization, the denoising network is given a noisy target image (in our case a depth map),  $\mathbf{z}_t = \alpha_t \mathbf{x} + \sigma_t \epsilon$ , where  $\mathbf{x}$  is the noiseless target input (depth map),  $\epsilon \sim \mathcal{N}(0, I)$ ,  $t \sim \mathcal{U}(0, 1)$ ,  $\sigma_t^2 = 1 - \alpha_t^2$ , and  $\alpha_t > 0$  is computed with a pre-determined noise schedule, and the denoising network predicts  $v \equiv \alpha_t \epsilon - \sigma_t \mathbf{x}$ . From the output of the denoising network, i.e.,  $v_\theta(\mathbf{z}_t, \mathbf{y}, t)$ , where  $\mathbf{y}$  is an optional conditioning signal (RGB image in this case), one obtains an estimate of  $\mathbf{x}$  at step  $t$ , i.e.,  $\hat{\mathbf{x}}_t = \alpha_t \mathbf{z}_t - \sigma_t v_\theta(\mathbf{z}_t, \mathbf{y}, t)$ , and the corresponding estimate of the noise, denoted  $\hat{\epsilon}_t$ . Under this parameterization, with a conventional L2 norm, the training objective is based on the expected ‘truncated SNR weighting’ loss, i.e.,  $\max(\|\mathbf{x} - \hat{\mathbf{x}}_t\|_2^2, \|\epsilon - \hat{\epsilon}_t\|_2^2)$  [39]. Motivated by the superior performance of the L1 loss in training DDVM [40] compared to the L2, we similarly employ a L1 loss for DMD as well, yielding the objective

$$\mathbb{E}_{\mathbf{x}, \mathbf{y}, t, \epsilon} [\max(\|\mathbf{x} - \hat{\mathbf{x}}_t\|_1, \|\epsilon - \hat{\epsilon}_t\|_1)] . \quad (1)$$

### 3.2. Joint indoor-outdoor modelling

Training a joint indoor-outdoor model can be difficult because of the large differences in depth distributions one finds in indoor and outdoor scenes. Much of the available indoor training data have depths up to 10m, while outdoor scenes include ground truth depths up to 80m. Further, training data is often lacking the variation in camera intrinsics needed for robustness to images from different cameras. Rather, many datasets are captured with a fixed camera. To mitigate these issues we propose three innovations, namely, the use of log depth, field of view augmentation, and field of view conditioning.

**Log depth.** Diffusion models usually model data distribution in  $[-1, 1]$ . One might convert metric depth to this range with linear scaling, i.e.,

$$d_{\text{lin}} = \text{normalize}(d_r / d_{\text{max}}) , \quad (2)$$

where  $d_r$  is the raw depth in meters,  $d_{\text{max}}$  is often taken to be 80m, to accommodate the usual outdoor depth range, and  $\text{normalize}(d) = \text{clip}(2 * d - 1, -1, 1)$ . This, however, allocates little representation capacity to indoor scenes (where depths are usually less than 10m).

Instead, we can allocate more representation capacity to indoor scenes with log-scaled depth ( $d_{\log}$ ) as the target for inference, i.e.,

$$d_{\log} = \text{normalize} \left( \frac{\log(d_r / d_{\min})}{\log(d_{\max} / d_{\min})} \right) , \quad (3)$$

where  $d_{\min}$  and  $d_{\max}$  denote the minimum and maximum supported depths (e.g., 0.5m and 80m). Empirically, we find log scaling to be remarkably beneficial.

**Field-of-view augmentation.** Because datasets for depth estimation often have little or no variation in the field of

view, it is easy for models to over-fit and thus generalize poorly to images with different camera intrinsics. To encourage models to generalize well to different fields of view, we propose to augment training data by cropping or uncropping to simulate diverse FOVs. While cropping is straightforward, for uncropping it is unclear how best to pad the enlarged image. Our preliminary experiments used generative uncropping with Palette [37], however, we found that padding the RGB image with Gaussian noise (mean-zero, variance 1) works as well, is simpler and more efficient.

For missing ground truth depth with uncropping augmentation, we adopt the approach in [40], using a combination of near-neighbor in-filling and step-unrolled denoising during training. It is shown in [40] that this technique is effective in coping with the inherent distribution shift between training and testing when ground truth data are noisy or incomplete.

**Field-of-view conditioning.** Metric depth estimation from a single image is ill-posed in the presence of unknown camera intrinsics, as depth scales inversely with the field-of-view. While one might hope that diversifying camera intrinsics through FOV augmentation will help generalization to different cameras, we and others [48] observe that it is not sufficient in itself. FOV augmentations do help simulate some variation in camera intrinsics, but variations in other factors, like focal length, are hard to simulate.

As a conditioning signal, to help disambiguate depth scale, we use  $\tan(\theta/2)$ , where  $\theta$  is the vertical FOV. We explored conditioning on the horizontal FOV as well, but that did not improve results substantially.

## 4. Experiments

### 4.1. Training data

DDVM [40] showed that using large amounts of diverse training data is important for generic models with no task-specific inductive biases. Here we follow the training strategy proposed in [40], initializing the model with unsupervised pre-training on ImageNet [12] and Places365 [52], with tasks proposed in [37]. This is followed by supervised pre-training on ScanNet [11], SceneNet-RGBD [31], and Waymo [45]. Unlike [40], we also include the DIML Indoor [10] dataset for more diversity. No FOV augmentation or conditioning is used for this pre-training stage.

For the final training stage we train on a mixture of NYU [42], Taskonomy [51], KITTI [19] and nuScenes [7]. At this stage we apply FOV augmentation to NYU, KITTI and nuScenes, but not Taskonomy as it is large and has substantial FOV diversity and also add the FOV conditioning. Finally, to enable fair comparisons with the current SOTA ZoeDepth [5] model, we also train a model solely from NYU and KITTI, like ZoeDepth.

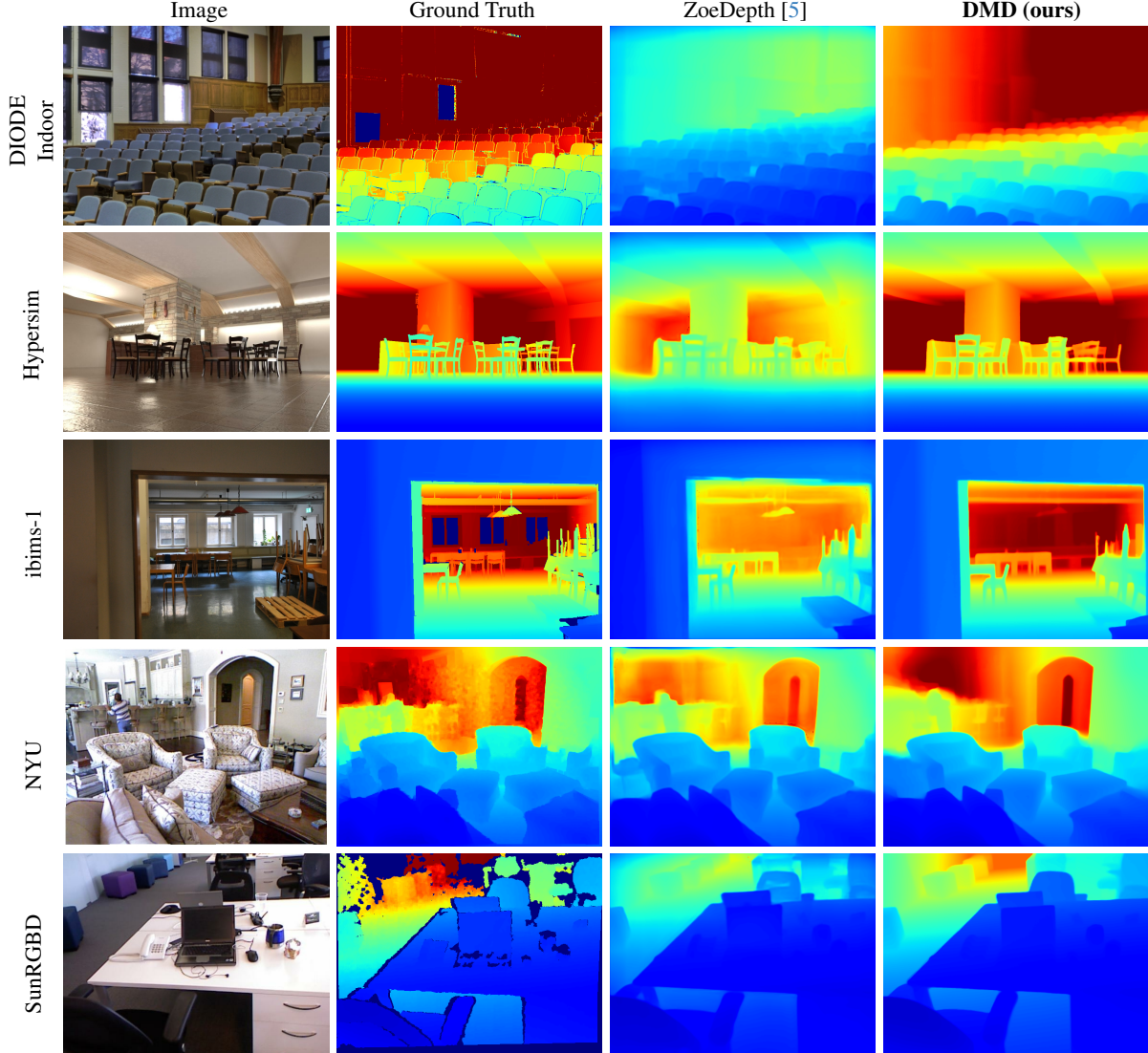


Figure 2. Qualitative comparison between our method and ZoeDepth [5] on indoor scenes. Unlike ZoeDepth, our method estimates depths at more accurate scale over diverse datasets.

Method	SUN RGB-D			iBims-1 Benchmark			DIODE Indoor			HyperSim		
	$\delta_1 \uparrow$	$REL \downarrow$	$RMSE \downarrow$	$\delta_1 \uparrow$	$REL \downarrow$	$RMSE \downarrow$	$\delta_1 \uparrow$	$REL \downarrow$	$RMSE \downarrow$	$\delta_1 \uparrow$	$REL \downarrow$	$RMSE \downarrow$
BTS [29]	0.740	0.172	0.515	0.538	0.231	0.919	0.210	0.418	1.905	0.225	0.476	6.404
AdaBins [3]	0.771	0.159	0.476	0.555	0.212	0.901	0.174	0.443	1.963	0.221	0.483	6.546
LocalBins [4]	0.777	0.156	0.470	0.558	0.211	0.880	0.229	0.412	1.853	0.234	0.468	6.362
NeWCRFs [50]	0.798	0.151	0.424	0.548	0.206	0.861	0.187	0.404	1.867	0.255	0.442	6.017
ZoeD-M12-NK [5]	0.856	0.123	0.356	0.615	0.186	0.777	0.386	0.331	1.598	0.274	0.419	5.830
<b>DMD-NK</b>	0.914	0.109	0.306	0.801	0.130	0.563	<b>0.402</b>	0.298	1.407	0.356	0.382	5.527
<b>DMD-MIX</b>	<b>0.930</b>	<b>0.091</b>	<b>0.275</b>	<b>0.859</b>	<b>0.118</b>	<b>0.447</b>	0.380	<b>0.291</b>	<b>1.292</b>	<b>0.497</b>	<b>0.318</b>	<b>4.394</b>

Table 1. **Zero-shot results** on unseen indoor datasets (evaluated at pixels with GT depth less 8m for SUN RGB-D, 10m for iBims-1 and DIODE Indoor, and 80m for Hypersim). **Best** and second-best results are highlighted. Trained on the same data (NYU and KITTI), DMD-NK outperforms ZoeD-M12-NK. With more data (Taskonomy and nuScenes), DMD-MIX outperforms by a much larger margin.

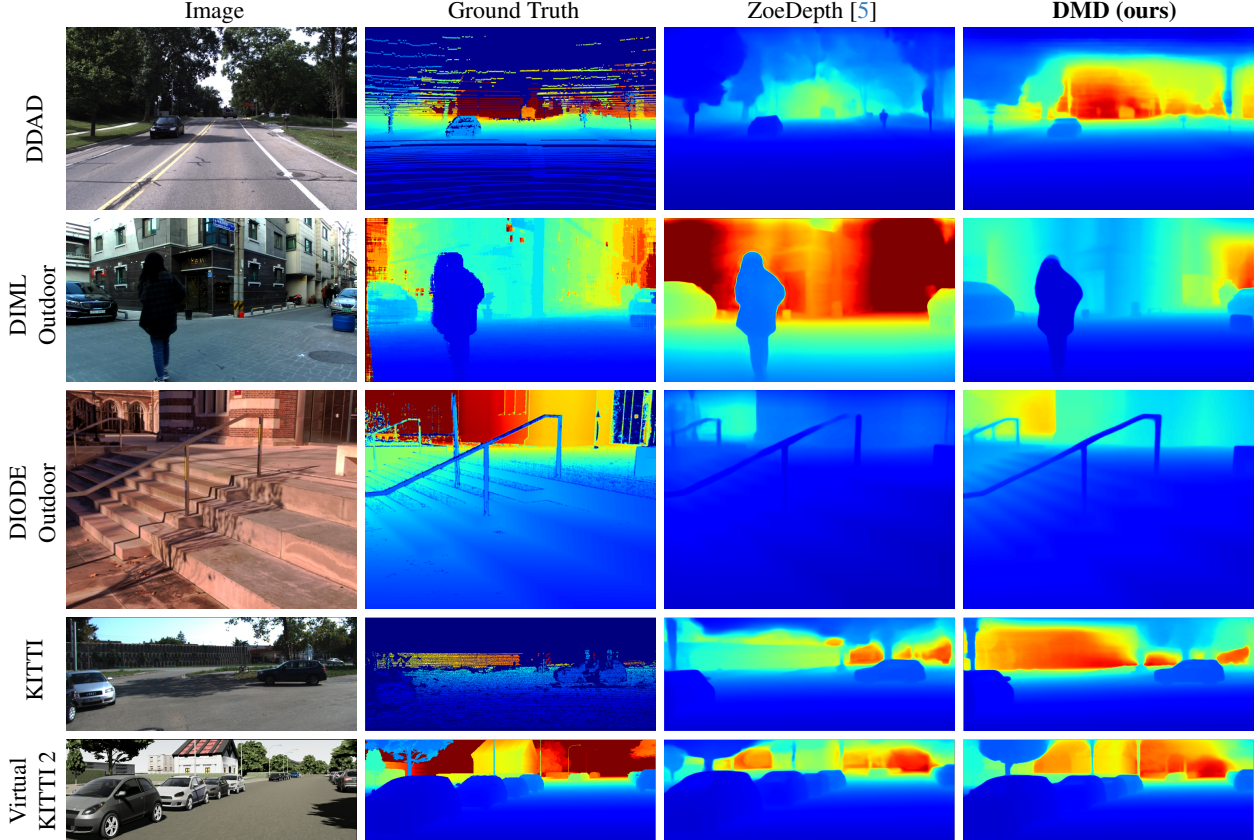


Figure 3. Qualitative comparison between DMD and ZoeDepth [5] on outdoor scenes. Compared with ZoeDepth [5], our method is able to estimate a more accurate depth scale.

Method	Virtual KITTI 2			DDAD			DIML Outdoor			DIODE Outdoor		
	$\delta_1 \uparrow$	REL $\downarrow$	RMSE $\downarrow$	$\delta_1 \uparrow$	REL $\downarrow$	RMSE $\downarrow$	$\delta_1 \uparrow$	REL $\downarrow$	RMSE $\downarrow$	$\delta_1 \uparrow$	REL $\downarrow$	RMSE $\downarrow$
BTS [29]	0.831	0.115	5.368	0.805	0.147	7.550	0.016	1.785	5.908	0.171	0.837	10.48
AdaBins [3]	0.826	0.122	5.420	0.766	0.154	8.560	0.013	1.941	6.272	0.161	0.863	10.35
LocalBins [4]	0.810	0.127	5.981	0.777	0.151	8.139	0.016	1.820	6.706	0.170	0.821	10.27
NeWCRFs [50]	0.829	0.117	5.691	0.874	0.119	6.183	0.010	1.918	6.283	0.176	0.854	9.228
ZoeD-M12-NK [5]	0.850	0.105	5.095	0.824	0.138	7.225	0.292	0.641	3.610	<b>0.208</b>	0.757	<b>7.569</b>
DMD-NK	0.872	0.093	4.828	0.842	0.122	6.740	0.544	0.300	2.522	0.162	0.627	9.577
DMD-MIX	<b>0.890</b>	<b>0.092</b>	<b>4.387</b>	<b>0.907</b>	<b>0.108</b>	<b>5.365</b>	<b>0.602</b>	<b>0.190</b>	<b>2.089</b>	0.187	<b>0.553</b>	8.943

Table 2. **Zero-shot results** on four unseen outdoor datasets. **Best** and **second-best** results are highlighted. Following pre-training, DMD-NK is trained on NYUv2 and KITTI, while DMD-MIX adds Taxonomy and NuScenes for training. Using the same fine-tuning data, DMD-NK outperforms ZoeD-M12-NK on all benchmarks except DIODE Outdoor where it outperforms on REL but is behind on other metrics. DMD-MIX shows further performance improvements over DMD-NK with the expanded training mixture.

Experiment	Indoors						Outdoors				
	NYU	SunRGBD	DIODE Indoor	ibims-1	Hypersim	KITTI	DIML Outdoor	DIODE Outdoor	Virtual KITTI 2	DDAD	
REL	Linear scaling	0.082	<b>0.108</b>	0.324	0.146	0.398	0.056	0.467	0.630	<b>0.092</b>	<b>0.122</b>
	Log scaling	<b>0.076</b>	0.109	<b>0.298</b>	<b>0.130</b>	<b>0.382</b>	<b>0.055</b>	<b>0.300</b>	<b>0.628</b>	0.093	<b>0.122</b>
RMS	Linear scaling	0.340	0.314	1.526	0.612	5.693	<b>2.516</b>	3.126	10.129	<b>4.788</b>	<b>6.288</b>
	Log scaling	<b>0.313</b>	<b>0.306</b>	<b>1.407</b>	<b>0.563</b>	<b>5.527</b>	2.527	<b>2.522</b>	<b>9.577</b>	4.828	6.740

Table 3. Ablation showing that log depth improves quantitative performance on indoor datasets which is understandable since log-scaling increases the share of representation capacity allocated to shallow depths.

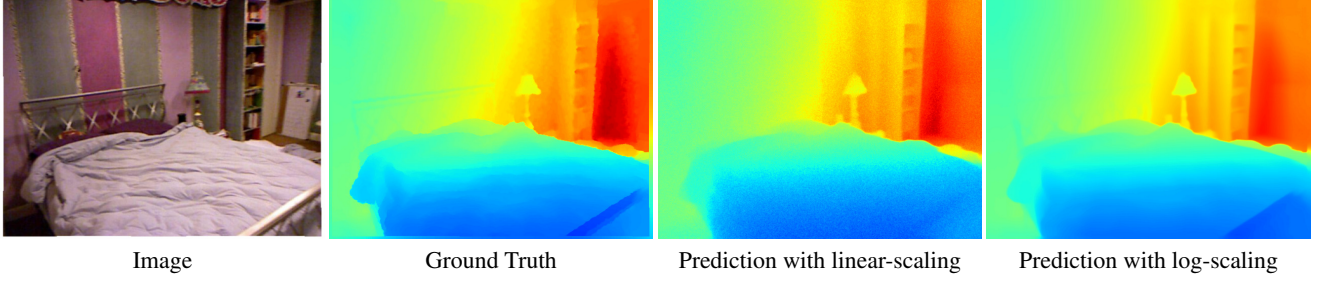


Figure 4. Linearly scaling depth leads to noisy predictions for images with shallow depth. See Section 3.2 for more details. Predicting depth in a log-scale fixes this. Note that here we use a max depth of 5 meters for better visualization.

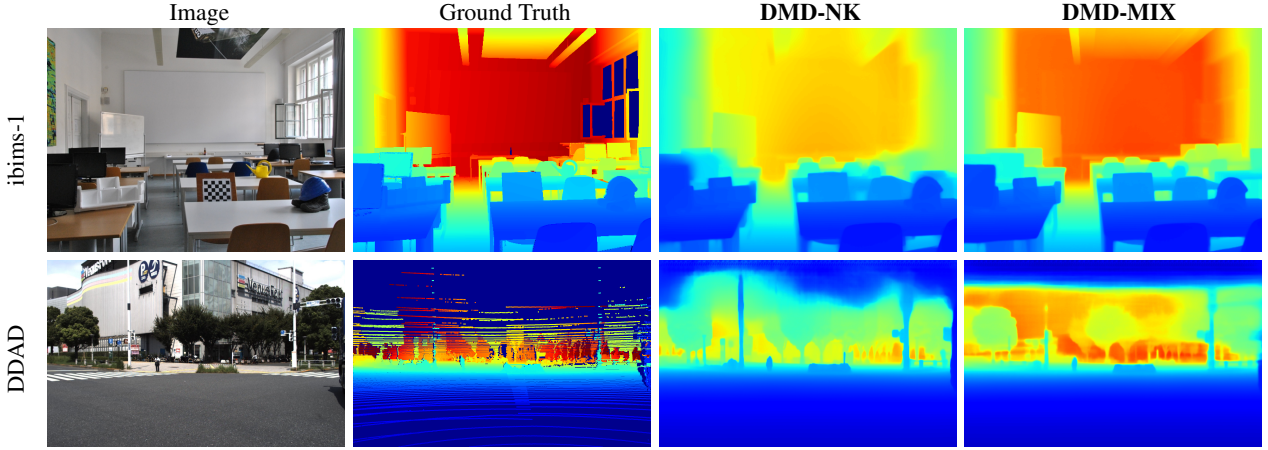


Figure 5. Qualitative comparison between DMD-NK (fine-tuned on NYU and KITTI) and DMD-MIX (fine-tuned on KITTI, NYU, nuScenes, and Taskonomy). DMD-MIX further improves depth scale estimation as well as fine details on depth boundaries.

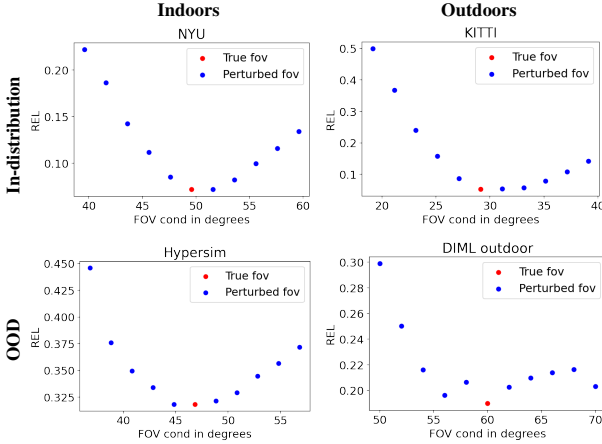


Figure 6. Plots showing the effect of perturbing the FOV during inference. Optimal performance is at or near the true FOV. Performance degrades with larger perturbation.

## 4.2. Design choices

**Denoiser Architecture.** We adopt the modifications of the *Efficient U-Net* [38] proposed in DDVM [40], with one further modification to support FOV conditioning. The FOV embedding, like the timestep embedding, is constructed by

first building a sin-cos positional embedding [47] followed by linear projection. The sum of these two embeddings is used to modulate different layers of the denoiser backbone using FiLM [33] layers. Following [5] we train at a resolution of  $384 \times 512$ . The predicted depth maps are resized to the ground-truth resolution for evaluation, following prior work [5]. Other training hyper-parameters such as the batch size and optimizer details are like those in [40].

**Augmentations.** In addition to the FOV augmentation (Sec. 3.2) we use random horizontal flip augmentation, like many prior works.

**Sampler.** We use the DDPM [23] sampler with eight denoising steps for indoor datasets. For outdoor datasets we find that two denoising steps suffice. We report results using a mean of eight samples, following [40]; as shown in Table 6, sample averaging leads to improved performance.

**Evaluation.** We adopt the evaluation protocol of ZooDepth [5]. We report in-distribution performance on the NYU [42] and KITTI [19] datasets, and generalization performance on eight unseen datasets [5], namely, SunRGBD [44], iBims-1 [44], DIODE Indoor [46], Hypersim [36] for indoors, and Virtual KITTI 2 [6], DDAD [20], DIML Outdoor [10],

Method	NYU						KITTI						
	$\delta_1 \uparrow$	$\delta_2 \uparrow$	$\delta_3 \uparrow$	$REL \downarrow$	$RMS \downarrow$	$\log_{10} \downarrow$	$\delta_1 \uparrow$	$\delta_2 \uparrow$	$\delta_3 \uparrow$	$REL \downarrow$	$Sq\text{-}rel \downarrow$	$RMS \downarrow$	$RMS \log \downarrow$
<i>Domain-specific models:</i>													
BTS [29]	0.885	0.978	0.994	0.110	0.392	0.047	0.956	0.993	0.998	0.059	0.245	2.756	0.096
DPT [35]	0.904	0.988	0.998	0.110	0.357	0.045	0.959	0.995	0.999	0.062	–	2.573	0.092
AdaBins [3]	0.903	0.984	0.997	0.103	0.364	0.044	0.964	0.995	0.999	0.058	0.190	2.360	0.088
NeWCRFs [50]	0.922	0.992	0.998	0.095	0.334	0.041	0.974	0.997	0.999	0.052	0.155	2.129	0.079
BinsFormer [30]	0.925	0.989	0.997	0.094	0.330	0.040	0.974	0.997	0.999	0.052	0.151	2.098	0.079
PixelFormer [1]	0.929	0.991	0.998	0.090	0.322	0.039	0.976	0.997	0.999	0.051	0.149	2.081	0.077
IEBIns [41]	0.936	0.992	0.998	0.087	0.314	0.038	0.978	0.998	0.999	0.050	0.142	2.011	0.075
MIM [49]	0.949	0.994	0.999	0.083	0.287	0.035	0.977	0.998	1.000	0.050	0.139	1.966	0.075
DDVM [40]	0.946	0.987	0.996	0.074	0.315	0.032	0.965	0.994	0.998	0.055	0.292	2.613	0.089
<i>Joint indoor-outdoor models:</i>													
ZoeD-M12-NK	<b>0.953</b>	<b>0.995</b>	<b>0.999</b>	0.077	<b>0.277</b>	0.033	0.966	0.993	0.996	0.057	0.204	<b>2.362</b>	0.087
<b>DMD-NK</b>	0.944	0.986	0.996	0.076	0.313	0.033	0.964	0.994	<b>0.999</b>	0.055	0.219	2.527	0.087
<b>DMD-MIX</b>	<b>0.953</b>	0.989	0.996	<b>0.072</b>	0.296	<b>0.031</b>	<b>0.967</b>	<b>0.995</b>	<b>0.999</b>	<b>0.053</b>	<b>0.203</b>	2.411	<b>0.084</b>

Table 4. **In-domain results** showing better relative error than ZoeDepth for our models on both the NYU and KITTI datasets. **Best** results (amongst indoor-outdoor models only) are bolded. For reference, we provide results for models trained separately for the indoor and outdoor domains showing that our results are competitive despite being a more general model.

Metric	Experiment	Indoors						Outdoors					
		NYU	SunRGBD	DIODE Indoor	ibims-1	Hypersim	KITTI	DIML	Outdoor	DIODE Outdoor	Virtual KITTI 2	DDAD	
REL	No FOV cond	0.081	0.116	0.316	0.18	0.400	0.057	1.257		<b>0.613</b>	0.100	<b>0.121</b>	
	With FOV cond	<b>0.076</b>	<b>0.109</b>	<b>0.298</b>	<b>0.130</b>	<b>0.382</b>	<b>0.055</b>	<b>0.300</b>		0.628	<b>0.093</b>	0.122	
RMS	No FOV cond	0.319	0.325	1.474	0.712	<b>5.196</b>	2.574	5.382		<b>8.582</b>	5.021	6.826	
	With FOV cond	<b>0.313</b>	<b>0.306</b>	<b>1.407</b>	<b>0.563</b>	5.527	<b>2.527</b>	<b>2.522</b>		9.577	<b>4.828</b>	<b>6.740</b>	

Table 5. Depth errors for models trained with and without field-of-view conditioning. Results shows that FOV conditioning provides a substantial boost in performance. DIML Outdoor benefits the most, which is understandable given its large FOV, for which generalization is a major challenge for simple FOV augmentation.

DIODE Outdoor [46] for outdoors. We closely follow the evaluation protocol, including depth ranges and cropping, used in [5] and report results using the standard error and accuracy metrics that are used in literature.

### 4.3. Results

**Zero-shot.** Tables 1 and 2 report *zero-shot* performance on eight OOD datasets. DMD-NK permits fair comparison with ZoeDepth, as both are fine-tuned on NYU and KITTI. With these datasets, DMD outperforms ZoeDepth across all but DIODE Outdoor, where DMD-NK outperforms ZoeDepth on relative error but not RMSE and  $\delta_1$ . Importantly, but perhaps not surprisingly, further performance improvements are obtained by fine-tuning on larger amounts of data. Our variant trained on a mixture with KITTI, NYU, nuScenes, and Taskonomy, dubbed DMD-MIX, generalizes much better on OOD test data, establishing an even stronger new state of the art.

Figures 2 and 3 visualize qualitative comparison between DMD and ZoeDepth on indoor and outdoor datasets respectively. Our method captures more accurate metric-scale depth with both indoor and outdoor scenes. Fig. 5 illustrates the qualitative differences in depth maps from

DMD-NK and DMD-MIX. By virtue of training on a larger dataset, DMD-MIX significantly improves the depth scale and fine-grained depth details near object boundaries.

**In-distribution.** Table 4 reports results on the KITTI and NYU datasets. On KITTI, DMD-MIX outperforms ZoeDepth on all metrics except RMSE where it is competitive. On NYU DMD-MIX substantially outperforms ZoeDepth on relative error and is competitive on other metrics. Interestingly, DMD-MIX outperforms DMD-NK on in-distribution data.

### 4.4. Ablations

We next consider several ablations to test different components of the model, all with DMD-NK for expedience.

**Log vs linearly scaled depth.** Table 3 shows that parameterizing depth in log scale (Sec. 3.2) improves quantitative performance. As expected, this is beneficial for datasets of indoor scenes and also for datasets of outdoor scenes with shallower depths, like DIML Outdoor and DIODE Outdoor. Furthermore, as shown in Fig. 4, using linear-scaling leads to noise artifacts in the depth estimates for indoor scenes

Metric	# samples	Indoors					Outdoors							
		NYU	SunRGBD	DIODE	Indoor	ibims-1	Hypersim	KITTI	DIML	Outdoor	DIODE	Outdoor	Virtual	KITTI 2
REL	1	0.077	0.110	0.304	0.135	0.383	<b>0.055</b>	0.311	0.634	<b>0.093</b>	<b>0.122</b>			
	8	<b>0.076</b>	<b>0.109</b>	<b>0.298</b>	<b>0.130</b>	<b>0.382</b>	<b>0.055</b>	<b>0.300</b>	<b>0.628</b>	<b>0.093</b>	<b>0.122</b>			
RMS	1	0.321	0.311	1.426	0.579	<b>5.521</b>	2.544	2.572	9.602	4.842	6.755			
	8	<b>0.313</b>	<b>0.306</b>	<b>1.407</b>	<b>0.563</b>	5.527	<b>2.527</b>	<b>2.522</b>	<b>9.577</b>	<b>4.828</b>	<b>6.740</b>			

Table 6. Averaging multiple samples leads to small but consistent improvement on both REL and RMS.

Metric	Experiment	Indoors					Outdoors							
		NYU	SunRGBD	DIODE	Indoor	ibims-1	Hypersim	KITTI	DIML	Outdoor	DIODE	Outdoor	Virtual	KITTI 2
REL	No FOV aug or cond	<b>0.074</b>	0.124	0.337	0.180	0.479	<b>0.055</b>	1.399	<b>0.615</b>	0.095	<b>0.116</b>			
	W/ FOV aug and cond	0.076	<b>0.109</b>	<b>0.298</b>	<b>0.130</b>	<b>0.382</b>	<b>0.055</b>	<b>0.300</b>	0.628	<b>0.093</b>	0.122			
RMS	No FOV aug or cond	<b>0.310</b>	0.348	1.535	0.722	<b>5.247</b>	2.597	5.919	<b>8.529</b>	4.874	<b>6.476</b>			
	W/ FOV aug and cond	0.313	<b>0.306</b>	<b>1.407</b>	<b>0.563</b>	5.527	<b>2.527</b>	<b>2.522</b>	9.577	<b>4.828</b>	6.740			

Table 7. Ablation showing that training without FOV augmentations and conditioning hurts generalization to out-of-domain data due to overfitting on the training data intrinsics.

	REL ↓		RMSE ↓	
	NYU	KITTI	NYU	KITTI
ZoeDepth Auto Router	0.102	0.075	0.377	<b>2.584</b>
Ours no fov aug / cond	<b>0.074</b>	<b>0.055</b>	<b>0.310</b>	2.597

Table 8. Comparison against ZoeDepth without scene type supervision. ZoeDepth performance degrades significantly when the scene type (indoor or outdoor) is not provided. DMD learns well without such supervision.

Num denoising steps	NYU		KITTI	
	$\epsilon$	$v$	$\epsilon$	$v$
1	2.374	0.077	0.596	0.056
4	1.484	0.075	0.406	0.055
16	0.409	0.074	0.141	0.055
64	0.077	0.074	0.056	0.055

Table 9. Comparison of relative error on NYU and KITTI for models trained with  $\epsilon$ - and  $v$ - parameterization. Both are fine-tuned on NYU and KITTI without FOV augmentation or conditioning.

which is resolved with log-depth parameterization.

**Field-of-view conditioning.** Table 5 shows that FOV conditioning achieves the best performance. Fig. 6 perturbs the conditioning FOV signal during inference, showing that optimal performance occurs at or close to the true FOV.

**No FOV augmentation or conditioning.** ZoeDepth found that without scene-type supervision for the experts (i.e., *Auto Router*), ZoeDepth’s performance degrades, even for in-domain data. To compare against ZoeDepth in this setting, we fine-tune a model on NYU and KITTI without FOV augmentations or conditioning. Interestingly, DMD performs relatively well in this setting for in-domain data (Table 8). Nevertheless, as shown in Table 7, OOD performance is better with FOV augmentation and conditioning.

**$\epsilon$  vs  $v$  diffusion parameterization.** Inference latency is a concern with diffusion models for vision. DDVM [40], for example, uses 128 denoising steps for depth estimation which can be prohibitive. We find that using the  $v$ -parameterization dramatically reduces the number of denoising steps required for good performance. As shown in Table 9,  $\epsilon$ -parameterization requires 64 denoising steps to match the performance of a model with  $v$ -parameterization using only 1 denoising step. Intuitively,  $v$ -parameterization

ensures that the model accurately recovers the signal at both ends of the noise schedule, unlike  $\epsilon$ -parameterization where estimating the noise is easy for low SNR inputs.

## 5. Conclusion

We propose a generic diffusion-based monocular metric depth generator with no task-specific inductive biases and no specialized architectures for handling diverse indoor and outdoor scenes. Our log-scale depth parameterization adequately allocates representation capacity to different depth ranges. We advocate augmenting the FOV of training data through simple cropping/uncropping to enable generalization to fields-of-view beyond those in the training datasets and show that simply uncropping with noise padding is effective for simulating a larger FOV. We find that conditioning on the FOV is essential for disambiguating depth-scale. We further propose a new fine-tuning dataset mixture that dramatically improves performance. With these innovations combined, we establish a new state-of-the-art outperforming the prior work of ZoeDepth across all zero-shot and in-domain datasets by a substantial margin.

## Acknowledgements

We thank Jon Shlens, Kevin Swersky, Shekoofeh Azizi and Cristina Vasconcelos for their detailed feedback and help with figures. We also thank Ting Chen, Daniel Watson, Forrester Cole and others in Google DeepMind and Google Research for helpful discussions.

## References

- [1] Ashutosh Agarwal and Chetan Arora. Attention Attention Everywhere: Monocular depth prediction with skip attention. In *WACV*, 2023. [2](#) [7](#)
- [2] Manuel López Antequera, Pau Gargallo, Markus Hofinger, Samuel Rota Bulò, Yubin Kuang, and Peter Kontschieder. Mapillary planet-scale depth dataset. In *ECCV*, pages 589–604, 2020. [2](#)
- [3] Shariq Farooq Bhat, Ibraheem Alhashim, and Peter Wonka. AdaBins: Depth estimation using adaptive bins. In *CVPR*, pages 4009–4018, 2021. [2](#) [4](#) [5](#) [7](#)
- [4] Shariq Farooq Bhat, Ibraheem Alhashim, and Peter Wonka. LocalBins: Improving depth estimation by learning local distributions. In *ECCV*, pages 480–496, 2022. [4](#) [5](#)
- [5] Shariq Farooq Bhat, Reiner Birk, Diana Wofk, Peter Wonka, and Matthias Müller. ZoeDepth: Zero-shot transfer by combining relative and metric depth. *arXiv preprint arXiv:2302.12288*, 2023. [1](#) [2](#) [3](#) [4](#) [5](#) [6](#) [7](#) [11](#) [12](#)
- [6] Yohann Cabon, Naila Murray, and Martin Humenberger. Virtual KITTI 2, 2020. [6](#)
- [7] Holger Caesar, Varun Bankiti, Alex H. Lang, Sourabh Vora, Venice Erin Liong, Qiang Xu, Anush Krishnan, Yu Pan, Giacarlo Baldan, and Oscar Beijbom. nuScenes: A multimodal dataset for autonomous driving. In *CVPR*, 2020. [3](#)
- [8] Yuanzhouhan Cao, Zifeng Wu, and Chunhua Shen. Estimating depth from monocular images as classification using deep fully convolutional residual networks. *IEEE T-CSVT*, 28(11):3174–3182, 2017. [2](#)
- [9] Ting Chen, Lala Li, Saurabh Saxena, Geoffrey Hinton, and David J. Fleet. A generalist framework for panoptic segmentation of images and videos. In *ICCV*, 2023. [2](#)
- [10] Jaehoon Cho, Dongbo Min, Youngjung Kim, and Kwanghoon Sohn. DIML/CVL RGB-D dataset: 2M RGB-D images of natural indoor and outdoor scenes. *arXiv preprint arXiv:2110.11590*, 2021. [3](#) [6](#)
- [11] Angela Dai, Angel X. Chang, Manolis Savva, Maciej Halber, Thomas Funkhouser, and Matthias Nießner. ScanNet: Richly-annotated 3D reconstructions of indoor scenes. In *CVPR*, 2017. [3](#)
- [12] Jia Deng, Wei Dong, Richard Socher, Li-Jia Li, Kai Li, and Li Fei-Fei. ImageNet: A large-scale hierarchical image database. In *CVPR*, pages 248–255, 2009. [3](#)
- [13] Prafulla Dhariwal and Alex Nichol. Diffusion models beat GANs on image synthesis. In *NeurIPS*, 2022. [2](#)
- [14] Yiqun Duan, Xianda Guo, and Zheng Zhu. DiffusionDepth: Diffusion denoising approach for monocular depth estimation. *arXiv preprint arXiv:2303.05021*, 2023. [2](#)
- [15] David Eigen and Rob Fergus. Predicting depth, surface normals and semantic labels with a common multi-scale convolutional architecture. In *ICCV*, pages 2650–2658, 2015. [2](#)
- [16] David Eigen, Christian Puhrsch, and Rob Fergus. Depth map prediction from a single image using a multi-scale deep network. In *NIPS*, 2014. [2](#)
- [17] Jose M. Facil, Benjamin Ummenhofer, Huizhong Zhou, Luis Montesano, Thomas Brox, and Javier Civera. CAM-Convs: Camera-Aware Multi-Scale Convolutions for Single-View Depth. In *CVPR*, 2019. [2](#)
- [18] Huan Fu, Mingming Gong, Chaohui Wang, Kayhan Batmanghelich, and Dacheng Tao. Deep ordinal regression network for monocular depth estimation. In *CVPR*, pages 2002–2011, 2018. [2](#)
- [19] Andreas Geiger, Philip Lenz, Christoph Stiller, and Raquel Urtasun. Vision meets Robotics: The KITTI dataset. *The International Journal of Robotics Research*, 32(11):1231–1237, 2013. [3](#) [6](#)
- [20] Vitor Guizilini, Rares Ambrus, Sudeep Pillai, Allan Raventos, and Adrien Gaidon. 3D packing for self-supervised monocular depth estimation. In *CVPR*, 2020. [6](#)
- [21] Vitor Guizilini, Igor Vasiljevic, Dian Chen, Rares Ambrus, and Adrien Gaidon. Towards zero-shot scale-aware monocular depth estimation. In *ICCV*, pages 9233–9243, 2023. [2](#)
- [22] Lei He, Guanghui Wang, and Zhanyi Hu. Learning depth from single images with deep neural network embedding focal length. *IEEE Transactions on Image Processing*, 27(9):4676–4689, 2018. [2](#)
- [23] Jonathan Ho, Ajay Jain, and Pieter Abbeel. Denoising Diffusion Probabilistic Models. *NeurIPS*, 2020. [2](#) [6](#)
- [24] Jonathan Ho, Chitwan Saharia, William Chan, David J. Fleet, Mohammad Norouzi, and Tim Salimans. Cascaded diffusion models for high fidelity image generation. *JMLR*, 2022. [2](#)
- [25] Yannick Hold-Geoffroy, Kalyan Sunkavalli, Jonathan Eisenmann, Matt Fisher, Emiliano Gambaretto, Sunil Hadap, and Jean-Francois Lalonde. A perceptual measure for deep single image camera calibration. In *CVPR*. IEEE, 2018. [12](#)
- [26] Yuanfeng Ji, Zhe Chen, Enze Xie, Lanqing Hong, Xihui Liu, Zhaoqiang Liu, Tong Lu, Zhenguo Li, and Ping Luo. DDP: Diffusion model for dense visual prediction. In *ICCV*, 2023. [2](#)
- [27] Linyi Jin, Jianming Zhang, Yannick Hold-Geoffroy, Oliver Wang, Kevin Blackburn-Matzen, Matthew Sticha, and David F. Fouhey. Perspective fields for single image camera calibration. In *CVPR*, 2023. [12](#)
- [28] Iro Laina, Christian Rupprecht, Vasileios Belagiannis, Federico Tombari, and Nassir Navab. Deeper depth prediction with fully convolutional residual networks. In *3DV*, pages 239–248, 2016. [2](#)
- [29] Jin Han Lee, Myung-Kyu Han, Dong Wook Ko, and Il Hong Suh. From big to small: Multi-scale local planar guidance for monocular depth estimation. *arXiv:1907.10326*, 2019. [4](#) [5](#) [7](#)
- [30] Zhenyu Li, Xuyang Wang, Xianming Liu, and Junjun Jiang. BinsFormer: Revisiting adaptive bins for monocular depth estimation. *arxiv:2204.00987*, 2022. [2](#) [7](#)

- [31] John McCormac, Ankur Handa, Stefan Leutenegger, and Andrew J. Davison. SceneNet RGB-D: Can 5M synthetic images beat generic imagenet pre-training on indoor segmentation? In *ICCV*, 2017. 3
- [32] Alex Nichol and Prafulla Dhariwal. Improved denoising diffusion probabilistic models. In *ICML*, 2021. 2
- [33] Ethan Perez, Florian Strub, Harm De Vries, Vincent Dumoulin, and Aaron Courville. FiLM: Visual Reasoning with a General Conditioning Layer . In *AAAI*, 2018. 6
- [34] René Ranftl, Katrin Lasinger, David Hafner, Konrad Schindler, and Vladlen Koltun. Towards robust monocular depth estimation: Mixing datasets for zero-shot cross-dataset transfer. *IEEE TPAMI*, 44(3):1623–1637, 2020. 1, 2
- [35] René Ranftl, Alexey Bochkovskiy, and Vladlen Koltun. Vision transformers for dense prediction. In *ICCV*, pages 12179–12188, 2021. 2, 7
- [36] Mike Roberts, Jason Ramapuram, Anurag Ranjan, Atulit Kumar, Miguel Angel Bautista, Nathan Paczan, Russ Webb, and Joshua M. Susskind. Hypersim: A photorealistic synthetic dataset for holistic indoor scene understanding. In *ICCV*, 2021. 6
- [37] Chitwan Saharia, William Chan, Huiwen Chang, Chris A. Lee, Jonathan Ho, Tim Salimans, David J. Fleet, and Mohammad Norouzi. Palette: Image-to-Image Diffusion Models. In *SIGGRAPH*, 2022. 3, 11
- [38] Chitwan Saharia, William Chan, Saurabh Saxena, Lala Li, Jay Whang, Emily Denton, Seyed Kamvar Seyed Ghasemipour, Burcu Karagol Ayan, S. Sara Mahdavi, Rapha Gontijo Lopes, Tim Salimans, Jonathan Ho, David J. Fleet, and Mohammad Norouzi. Photorealistic Text-to-Image Diffusion Models with Deep Language Understanding. In *NeurIPS*, 2022. 2, 6
- [39] Tim Salimans and Jonathan Ho. Progressive distillation for fast sampling of diffusion models. In *ICLR*, 2022. 2, 3
- [40] Saurabh Saxena, Charles Herrmann, Junhwa Hur, Abhishek Kar, Mohammad Norouzi, Deqing Sun, and David J. Fleet. The surprising effectiveness of diffusion models for optical flow and monocular depth estimation. In *NeurIPS*, 2023. 2, 3, 6, 7, 8
- [41] Shuwei Shao, Zhongcai Pei, Xingming Wu, Zhong Liu, Weihai Chen, and Zhengguo Li. IEBins: Iterative elastic bins for monocular depth estimation. In *NeurIPS*, 2023. 7
- [42] Nathan Silberman, Derek Hoiem, Pushmeet Kohli, and Rob Fergus. Indoor segmentation and support inference from RGBD images. In *ECCV*, pages 746–760, 2012. 3, 6
- [43] Jascha Sohl-Dickstein, Eric Weiss, Niru Maheswaranathan, and Surya Ganguli. Deep unsupervised learning using nonequilibrium thermodynamics. In *ICML*, pages 2256–2265, 2015. 2
- [44] Shuran Song, Samuel P. Lichtenberg, and Jianxiong Xiao. Sun RGB-D: A RGB-D scene understanding benchmark suite. In *CVPR*, pages 567–576, 2015. 6
- [45] Pei Sun, Henrik Kretzschmar, Xerxes Dotiwalla, Aurelien Chouard, Vijaysai Patnaik, Paul Tsui, James Guo, Yin Zhou, Yuning Chai, Benjamin Caine, Vijay Vasudevan, Wei Han, Jiquan Ngiam, Hang Zhao, Aleksei Timofeev, Scott Ettinger, Maxim Krivokon, Amy Gao, Aditya Joshi, Sheng Zhao, Shuyang Cheng, Yu Zhang, Jonathon Shlens, Zhifeng Chen, and Dragomir Anguelov. Scalability in perception for autonomous driving: Waymo open dataset. In *CVPR*, 2020. 3
- [46] Igor Vasiljevic, Nick Kolkin, Shanyi Zhang, Ruotian Luo, Haochen Wang, Falcon Z. Dai, Andrea F. Daniele, Mohammadreza Mostajabi, Steven Basart, Matthew R. Walter, and Gregory Shakhnarovich. DIODE: A Dense Indoor and Outdoor DEpth Dataset. *CoRR*, abs/1908.00463, 2019. 6, 7
- [47] Ashish Vaswani, Noam Shazeer, Niki Parmar, Jakob Uszkoreit, Llion Jones, Aidan N Gomez, Łukasz Kaiser, and Illia Polosukhin. Attention is all you need. *NIPS*, 2017. 6
- [48] Chengrui Wei, Meng Yang, Lei He, and Nanning Zheng. FS-Depth: Focal-and-scale depth estimation from a single image in unseen indoor scene. *arXiv preprint arXiv:2307.14624*, 2023. 3
- [49] Zhenda Xie, Zigang Geng, Jingcheng Hu, Zheng Zhang, Han Hu, and Yue Cao. Revealing the dark secrets of masked image modeling. In *CVPR*, 2023. 7
- [50] Weihao Yuan, Xiaodong Gu, Zuozhuo Dai, Siyu Zhu, and Ping Tan. Neural window fully-connected CRFs for monocular depth estimation. In *CVPR*, pages 3916–3925, 2022. 4, 5, 7
- [51] Amir Zamir, Alexander Sax, William Shen, Leonidas Guibas, Jitendra Malik, and Silvio Savarese. Taskonomy: Disentangling task transfer learning. In *CVPR*, 2018. 3
- [52] Bolei Zhou, Agata Lapedriza, Aditya Khosla, Aude Oliva, and Antonio Torralba. Places: A 10 million image database for scene recognition. *IEEE transactions on pattern analysis and machine intelligence*, 40(6):1452–1464, 2017. 3

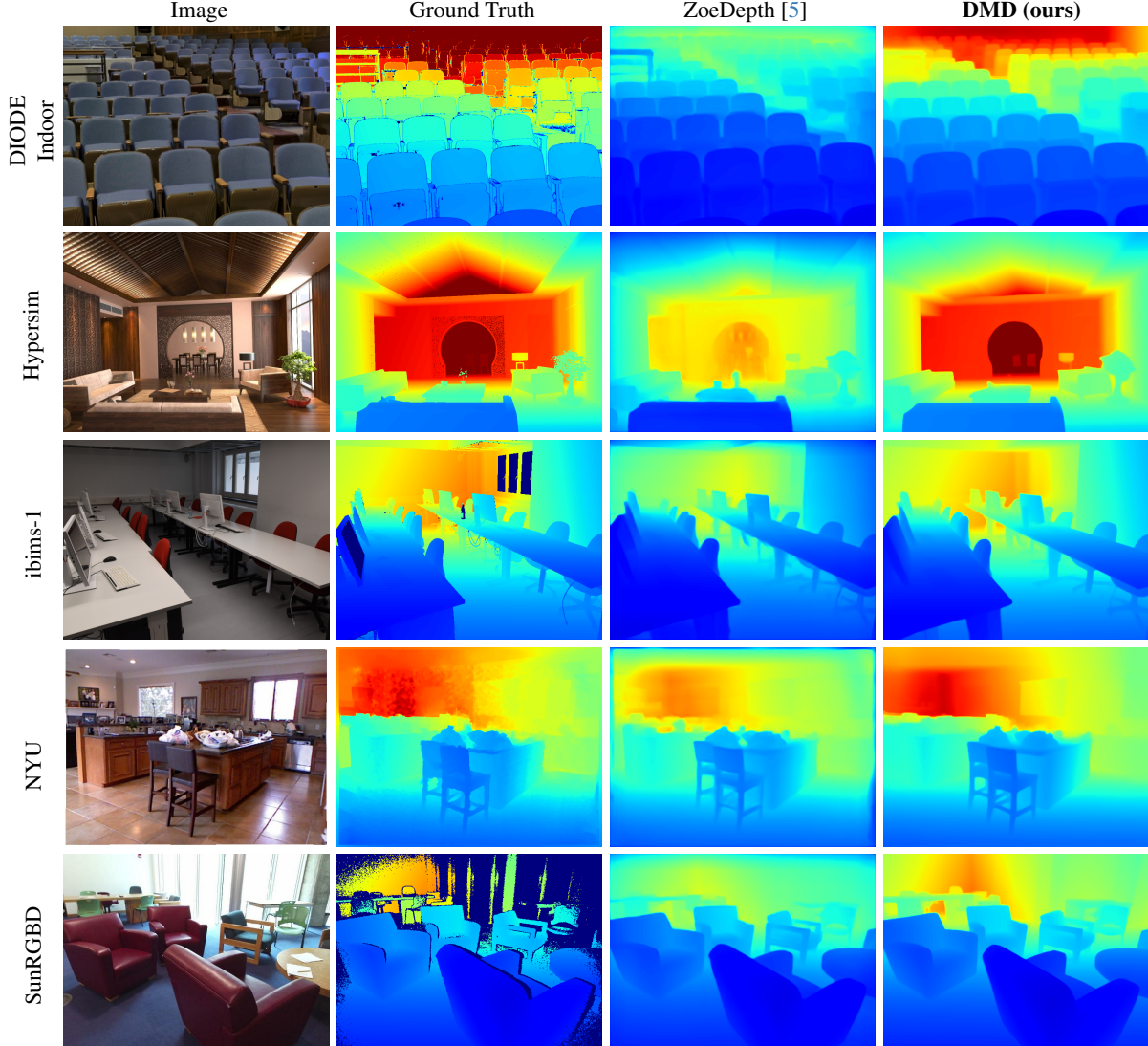


Figure 7. Qualitative comparison between our method and ZoeDepth [5] on indoor scenes. Compared with ZoeDepth, our method estimates depths at more accurate scale over diverse datasets.

## A. Additional qualitative examples

In Fig. 7 and Fig. 8, we provide additional qualitative comparison between DMD and ZoeDepth on indoor and outdoor datasets respectively. Our method consistently captures more accurate metric-scale depth in various indoor and outdoor scenes.

## B. Handling unknown field-of-view

While RGB camera intrinsics are available for most practical uses of monocular depth estimators (e.g. cell phones, robot platforms or self-driving cars), they may sometimes be unknown (e.g. internet images or generative imagery). One solution to handle the unknown FOV would be to estimate the camera intrinsics from the RGB image.

To test this, we train a simple model for predicting the vertical field-of-view (FOV). The model consists of the encoder of a pre-trained Palette [37] model followed by a spatial average pooling layer and a linear head that predicts a scalar. It is trained to regress to  $\tan(\theta/2)$ , where  $\theta$  is the vertical FOV, using a  $L_1$  loss. We train on a mix of the NYU and KITTI datasets employing the same FOV augmentation strategy as used for DMD-NK.

Table 10 compares the depth estimation performance of our models when using the estimated FOV versus the true FOV. Despite the simplistic design of our FOV estimator, the depth estimation performance when using the estimated FOV is competitive to that when using the true FOV, except for the DIML outdoor dataset, where the large error in FOV estimation leads to a much worse relative error for depth.

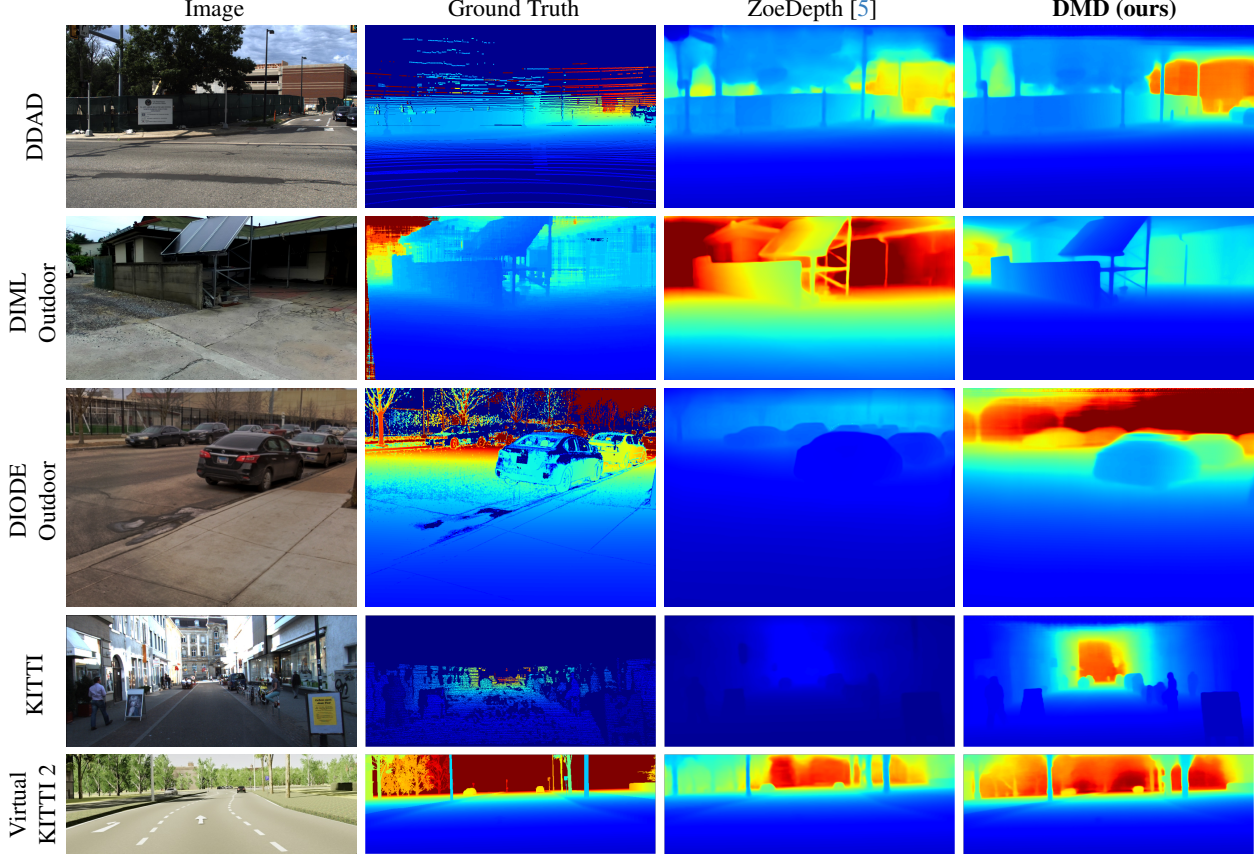


Figure 8. Qualitative comparison between DMD and ZoeDepth [5] on outdoor scenes. Compared with ZoeDepth [5], our method is able to estimate a more accurate depth scale.

Experiment	Indoors					Outdoors				
	NYU	SunRGBD	DIODE Indoor	ibims-1	Hypersim	KITTI	DIML Outdoor	DIODE Outdoor	Virtual KITTI 2	DDAD
DMD-NK true FOV	0.076	0.109	0.298	0.130	0.382	0.055	0.300	0.628	0.093	0.122
DMD-NK est. FOV	0.077	0.124	0.302	0.140	0.407	0.062	1.490	0.639	0.114	0.132
DMD-MIX true FOV	0.072	0.091	0.291	0.118	0.318	0.053	0.190	0.553	0.092	0.108
DMD-MIX est. FOV	0.072	0.136	0.291	0.114	0.361	0.061	1.049	0.560	0.131	0.119
FOV est. error (degrees)	1.520	5.114	0.735	2.339	4.224	0.842	27.998	3.459	4.142	4.384

Table 10. Comparison of relative error (REL) using an estimated (est.) FOV versus the true FOV. Even with a simple FOV estimator the depth estimation results using an estimated FOV are competitive to those with the true FOV, except for DIML Outdoor where our FOV estimator struggles to predict correct FOV as shown by the large error in FOV estimation.

This might be due to the significantly larger FOV of DIML outdoor, compared to other outdoor datasets, which could be challenging for our simple FOV regressor to generalize to. We hypothesize that incorporating more sophisticated camera intrinsic prediction models, such as those proposed by [25, 27], could lead to further improvements in FOV estimation accuracy, and thereby better metric depth estimates. However, we defer a thorough investigation of this approach to future work.

## C. Additional training details

We perform the first stage of supervised training for 1.5M steps with a learning rate of  $1 \times 10^{-4}$  and the second (final) stage for 50k steps with a learning rate of  $3 \times 10^{-5}$ . For the FOV augmentation in the second stage we randomly uniformly sample a scale in  $[0.8, 1.5]$  to crop/uncrop the image and depth maps.